Received 19 April 2023; revised 19 May 2023; accepted 7 June 2023. Date of publication 12 June 2023; date of current version 28 June 2023.
The review of this article was arranged by Editor P. Pavan.

Digital Object Identifier 10.1109/JEDS.2023.3285240

Analysis of Kink Effect in Short-Channel Floating Body PD-SOI MOSFETs

KYEONGJUN KIM AND SEONGHEARN LEE (Senior Member, IEEE)

Department of Electronic Engineering, Hankuk University of Foreign Studies, Yongin 17035, Gyeonggi, South Korea

CORRESPONDING AUTHOR: S. Lee (e-mail: shlee@hufs.ac.kr)

This work was supported in part by the Hankuk University of Foreign Studies Research Fund of 2023 and in part by the National Research Foundation of Korea (NRF) Grant funded by the Korea Government (MSIT) under Grant 2021R1A2C1095133.

ABSTRACT The origin of a greater decrease in kink drain voltage V_{kink} in floating body PD-SOI MOSFETs with gate lengths shorter than 0.35 μm is newly revealed. The V_{kink} formula as a function of the internal body voltage and I_{DS} is derived by combining the modified impact ionization multiplication factor with the body-source junction I-V equation. The parameters in this formula are extracted from the measured data of I_B vs. V_{BS} and $-I_B/I_{DS}$ vs. V_{DS} in the body contacted devices. By calculating the formula using the extracted parameters, it is newly found that a decrease of the drain-source saturation voltage at a shorter channel is a primary cause for the short-channel effect on V_{kink} reduction.

INDEX TERMS Kink effect, SOI MOSFET, short-channel, floating body, gate length dependence, parasitic BJT.

I. INTRODUCTION

As the gate length L_g is scaled down, high resistivity (HR) partially depleted (PD) silicon-on-insulator (SOI) MOSFETs have been steadily investigated as a promising solution to overcome problems such as latch-up, soft errors, high off-state current, high power consumption, and threshold voltage roll-off that appear in existing bulk MOSFETs. Since much lower cross-coupling, cross-talk noise, and leakage current compared to bulk MOSFETs can be attained using a HR-SOI substrate [1], [2], [3], many studies on HR PD-SOI devices have been carried out in applications such as low-power system-on-chip.

However, when the high drain-source voltage V_{DS} is applied in the floating body (FB) PD-SOI MOSFET in Fig. 1(a), the impact ionization hole current I_{imp} generated in the pinch-off region flows to the body, causing the internal body voltage V_{Bi} rise according to the equation for the I-V characteristics of the body-source junction of the parasitic BJT. As V_{Bi} increases, the threshold voltage V_{TH} decreases, leading to an increase in the channel current I_{ch} that is so called "kink effect" [4], [5]

The previous study on the kink effect in the FB devices shows that the kink drain voltage V_{kink} (at which the I_{DS} starts to ramp) decreases as L_g is shorten and V_{kink} goes down to $0.55V$ as L_g is scaled down to $80nm$ [6]. Since a lower operating voltage is required according to the scaling-down of L_g, the V_{kink} reduction may be main problem in designing low-power ICs. Thus, the origin of this short-channel kink effect should be identified before developing a physical FB device model.

To analyze the L_g dependence on V_{kink}, an accurate impact ionization model is required, but the existing electric field driven impact ionization model [7], [8] cannot explain V_{kink}

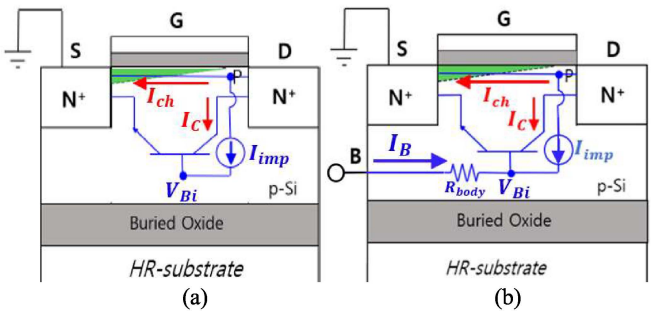

FIGURE 1. The cross-section of (a) FB PD-SOI n-MOSFET and (b) BCT PD-SOI n-MOSFET.

less than $E_g/q = 1.12\ V$. For explaining this sub-bandgap V_{kink}, the low-voltage thermally-assisted impact ionization multiplication factor M based on a simple activation energy model of $E_a = E_g - qV_{DS}$ has been reported [6], [9], but still does not contain any L_g related parameters. Thus, the low-voltage M equation needs to be modified for modeling the decrease of V_{kink} as L_g becomes shorter.

The impact ionization caused by the strong electric field in the pinch-off region is not related to the channel lateral electric field increased as L_g decreases. Since the avalanche breakdown voltage V_{br}, where I_{imp} becomes infinity, is directly affected by the common-emitter (source) current gain β of the parasitic BJT [7], it is commonly assumed that the decrease of V_{kink} as L_g is scaled down is mainly caused by the rise in β due to the reduction in L_g. However, β is not a direct parameter to determine V_{kink}, because the kink current is dominated by a channel current I_{ch} that is much higher than the collector current ($I_C = \beta I_{imp}$) of the parasitic BJT at $V_{kink} \ll V_{br}$ [8]. According to a basic kink effect mechanism, V_{kink} is determined by I_{DS}, M and the forward-biased body-source junction characteristics. However, a detail study to find the main cause of the reduction of V_{kink} has not been reported yet.

In this paper, we propose a modified L_g dependent M model and reveal the origin of the short-channel phenomenon that V_{kink} in FB PD-SOI n-MOSFETs decreases more sharply when L_g is less than 0.35 μm. To do this, we analyze in detail the short-channel effect based on the actual measurement data of the parasitic BJT in the body contact (BCT) PD-SOI MOSFETs in Fig. 1(b).

II. ANALYSIS OF THE KINK EFFECT

A. THEORETICAL ANALYSIS

As a high V_{DS} is applied in Fig. 1(a), I_{imp} is generated by impact ionization and I_{imp} flowing into the body-source junction of the parasitic BJT is expressed as:

$$I_{imp} = I_{bo}\left[\exp\left(\frac{qV_{Bi}}{\eta kT}\right) - 1\right] \tag{1}$$

where I_{bo} is the reverse saturation base current and η is the ideality factor of the body-source junction.

If body is floating, an increase of I_{imp} causes a rise of V_{Bi} according to (1), thus leading to a decrease in V_{TH} and a subsequent increase in I_{ch}. The drain-source current I_{DS} that is the sum of I_{ch} and I_C is multiplied by M in the drain pinch-off region. In this multiplication process, I_{imp} flowing into the body is defined by [5], [8]:

$$I_{imp} = (I_{ch} + I_C)(M - 1) = I_{DS}(M - 1) \tag{2}$$

In order to explain the V_{kink} values below E_g/q shown in Fig. 2, a low-voltage thermally-assisted M can be used as follows [6], [9]:

$$M - 1 = M_o \exp\left[-\frac{E_g - qV_{DS}}{kT}\right] \tag{3}$$

where M_0 is the value of $M - 1$ at $V_{DS} = E_g/q$.

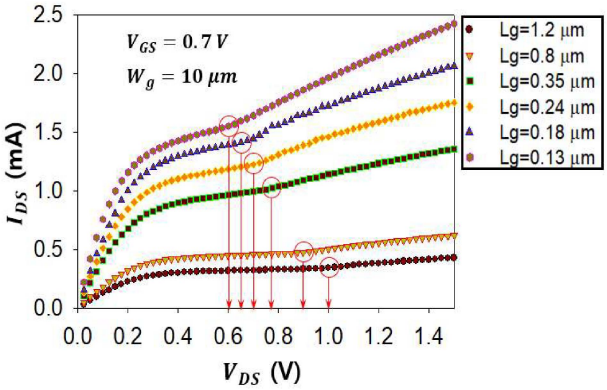

FIGURE 2. Measured $I_{DS} - V_{DS}$ characteristics of FB PD-SOI n-MOSFET for various L_g. The arrows indicate the V_{kink} values extracted for each L_g devices.

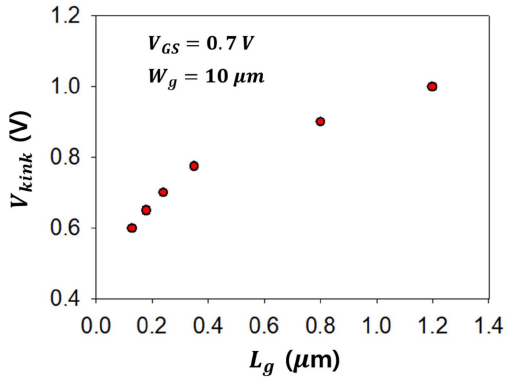

FIGURE 3. Measured V_{kink} vs. L_g of FB PD-SOI n-MOSFETs.

Combining (1)–(3) in the forward-biased junction at $V_{DS} = V_{kink}$, the following relationship is derived:

$$V_{kink} = \frac{V_{Bi}}{\eta} + \frac{kT}{q} ln\left(\frac{I_{bo}}{I_{DS}M_0}\right) + \frac{E_g}{q} \tag{4}$$

Since V_{kink} occurs at the same V_{Bi} needed for the initial reduction of V_{TH} regardless of L_g, the current ratio $I_{bo}/(I_{DS}M_0)$ in (4) mostly determines the L_g dependence of V_{kink}. Thus, V_{Bi}, M_0, I_{bo} and I_{DS} at V_{kink} for different L_g will be obtained by measuring I_{imp} vs. V_{BS} and I_{imp}/I_{DS} vs. V_{DS} in the next section.

B. MEASUREMENTS

The I-V curve of FB PD-SOI n-MOSFETs with $W_g = 10\ \mu m$ in Fig. 2 was measured while changing L_g from 0.13 to 1.2 μm. In Fig. 3, measured data for V_{kink} are plotted against L_g. The values of V_{kink} decrease with a steeper slope as L_g is shorter below 0.35 μm.

It is impossible to extract the parameter of (4) directly using the FB device without a body terminal. In this work, T-shape body contact (BCT) PD-SOI MOSFETs [8] with the same size as the FB device are used as test devices to measure the body-source junction I-V curve and I_{imp}. When $V_{DS} = V_{kink}$, the assumption is that I_{DS} in the FB device is similar to that in the BCT one because V_{kink} is an initial

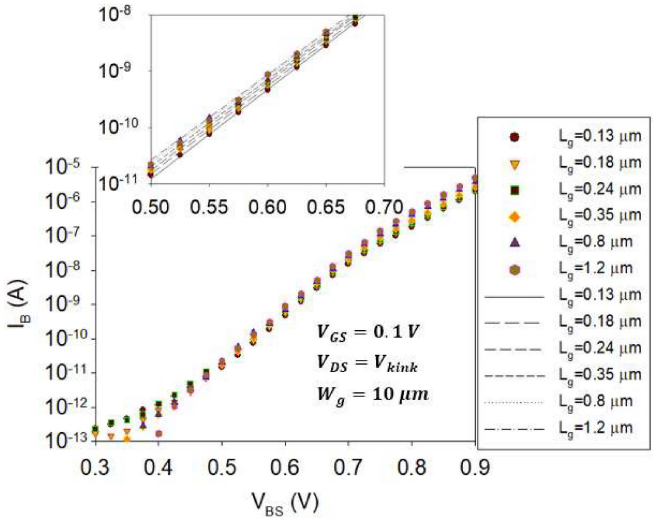

FIGURE 4. Measured data of I_B vs. V_{BS} at $V_{DS} = V_{kink}$ for BCT PD-SOI n-MOSFETs with various L_g. Fitted line plots for (1) are inserted inside.

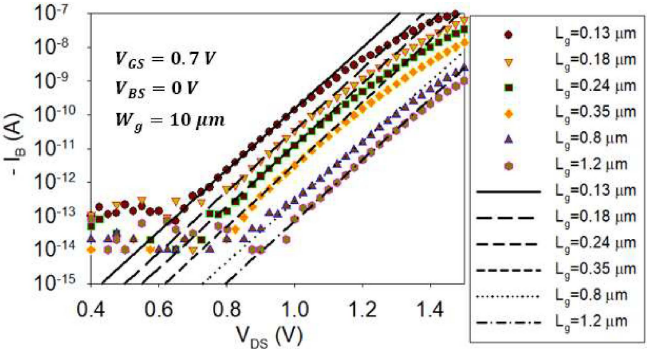

FIGURE 5. Measured data and fitted lines of (2) for $-I_B$ vs. V_{DS} at grounded V_{BS} for BCT PD-SOI n-MOSFETs with various L_g. The measured current of $-I_B$ flows out to the body terminal.

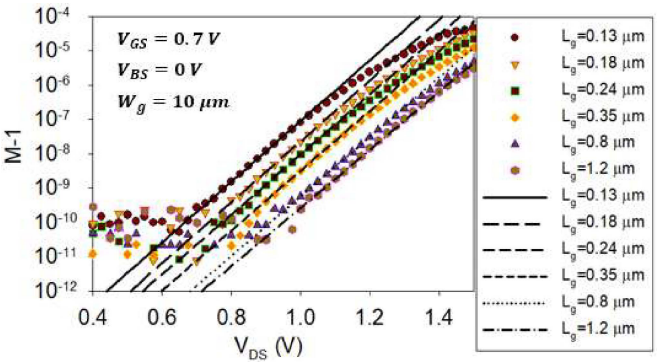

FIGURE 6. Measured data and fitted lines of (3) for $M-1$ vs. V_{DS} at grounded V_{BS} for BCT PD-SOI n-MOSFETs with various L_g.

voltage where I_{DS} begins to increase. Since $M-1$ remains unchanged between FB and BCT devices at V_{kink}, the body current measured in the grounded BCT device appears to be identical to that in the FB one. Thus, the measurement data of the BCT device can be used to extract the parameters of (4) in the FB device.

To obtain the junction IV characteristics of the parasitic BJT in the FB device, we need to apply the external V_{BS} in the BCT device and measure I_B in Fig. 1(b). Since $V_{Bi} \gg I_B R_{body}$, the external V_{BS} in the BCT device is equal to the internal V_{Bi} in the FB one. However, in Fig. 1(b), I_B flows into the base of the parasitic BJT and is added to I_{imp} that increases due to the rise of I_{ch} in (2) at V_{kink} in the BCT device. Thus, to accurately obtain the actual junction I-V characteristics of the parasitic BJT, I_B is measured at $V_{GS} < V_{TH}$ where I_{imp} of the BCT device in (2) is negligible in comparison to I_B because I_{ch} doesn't flow.

Fig. 4 shows that the measured I_B vs. V_{BS} for $L_g = 0.13 \sim 1.2\mu m$ when $V_{DS} = V_{kink}$. In the V_{BS} range above $1V$, it shows the slopes of $log(I_B)$ gradually decreases due to a high body resistance in the BCT devices. However, the leakage component caused by interface charges in the depletion region of the source junction just under gate oxide exists in the range of I_B below $1pA$. This leakage current disappears in the kink effect range when $V_{GS} > V_{TH}$ because of the channel formation under the gate oxide. Thus, $log(I_{bo})$ is determined from the y-intercept of the linear fitting lines of $log(I_B)$ vs. V_{BS} for (1) above $0.5V$ without the leakage in Fig. 4. When L_g is shorter, I_{bo} decreases because the recombination of the neutral body region decreases in the parasitic BJT.

In Fig. 5, $I_B(\approx -I_{imp})$ is measured while increasing V_{DS} in the BCT devices with $L_g = 0.13 \sim 1.2\mu m$. Also, the logarithmic equation of (2) combined with (3) is linearly fitted to $log(-I_B)$ data vs. V_{DS} for various L_g. The y-intercepts of the fitted $log(-I_B)$ lines are shown to increase with the decrease of L_g. The $M-1$ defined as $-I_B/I_{DS}$ in (2) is measured with varying V_{DS} in Fig. 6, but it was still observed that the y-intercepts increase with decreasing L_g. This indicates that other L_g dependent parameters should be introduced in (3).

III. IMPACT IONIZATION MODELING

In order to model the increase of $M-1$ with decreasing L_g in Fig. 6, the following procedure is performed in this section: First, a modified low-voltage thermally-assisted impact ionization multiplication factor model is proposed to explain the L_g dependence of $M-1$. Second, the impact ionization model parameters are directly extracted. Third, their influences of the extracted parameters on the measured $M-1$ are compared to identify the main cause responsible for the L_g dependence of $M-1$.

A. MODIFIED IMPACT IONIZATION MULTIPLICATION FACTOR MODEL

The reverse current in the drain-body junction is dominated by the generation current density [10] given by qn_iW/τ_g where n_i is the intrinsic concentration, W is the depletion width, and τ_g is the generation lifetime. Since $n_i \sim \exp[-\frac{E_g}{2kT}]$, E_a that is a minimum energy required to generate impact ionization carriers in the depletion region is reduced to $(E_g - qV_{DS})/2$ that is half of that proposed in a previous study [9]. This low E_a makes impact ionization possible at low energies below $E_g/2$.

Thus, $M-1$ of (3) should be modified by $M_o \exp[-\frac{E_g - qV_{DS}}{2kT}]$. This $2kT$ factor is directly verified by finding that the slopes of straight lines of $log(M-1)$ vs. V_{DS} in Fig. 6 are about half of the ideal slope of $S_I = q/[kT\ln(10)] = 16.7$ S in (3). Thus, by dividing S_I into the impact ideality factor m, it is possible to accurately model the measurement slope of $log(M-1)$.

Since the drain depletion region exists between the pinch-off point and the N+ drain region, the drain-source saturation voltage V_{DSAT} should be subtracted from V_{DS} to obtain an accurate voltage drop across both ends of the drain depletion region. The inaccuracy resulting from the omission of V_{DSAT} increases when modeling the low V_{kink} of short-channel devices, where sub-band gap impact ionization occurs.

Thus, we newly propose the following improved equation:

$$M-1 = M_0 \exp\left\{\frac{[q(V_{DS}-V_{DSAT})-E_g]}{mkT}\right\} \quad (5)$$

Taking a logarithmic function into both sides of (5) leads to:

$$log(M-1) = \frac{S_I}{m}V_{DS} - \frac{S_I}{m}\left(V_{DSAT} + \frac{E_g}{q}\right) + log(M_0) \quad (6)$$

In order to explain the L_g dependence that $M-1$ increases at shorter L_g in Fig. 6, it is necessary to satisfy the condition that V_{DSAT} decreases or M_0 increases at shorter L_g in (5). To check the validity of this condition, the L_g dependency of V_{DSAT} and M_0 is directly extracted in the next section.

B. EXTRACTION FOR V_{DSAT} AND M_0

To obtain the dependence of V_{DSAT} and M_0 on the short channel, V_{DSAT} in the BCT devices is directly extracted using the following method [11] based on a constant $M-1$ locus:

First, $M-1$ vs. V_{DS} is measured while varying V_{GS}, and then intersection points (V_{DSi}, V_{GSi}) of this curve at a constant $M-1$ are obtained. Next, I_{DSi} values corresponding to V_{DSi} and V_{GSi} are determined using a measured $I_{DS}-V_{DS}$ curve. This $I_{DSi}-V_{DSi}$ locus obtained at a constant $M-1$ is superimposed on the $I_{DS}-V_{DS}$ curve, and the x-intercept V_{DSx} is found by extrapolating the locus. Finally, the locus (V_{DSAT}, I_{DSAT}) as a function of V_{GS} is obtained by shifting the $I_{DSi}-V_{DSi}$ locus to pass through the origin using the parallel translation of $-V_{DSx}$.

Fig. 7 shows the extracted V_{DSAT} that decreases with a higher slope as L_g is shorten. These extracted values from the constant $M-1$ locus are shown to be a little bit smaller at shorter L_g than those estimated roughly from the boundary voltage between the linear and saturation regions in Fig. 2. Physically, as the channel length becomes shorter, V_{DSAT} decreases due to the carrier velocity saturation effect [12] and the reverse short-channel effect [13] leading to the increase of V_{TH} caused by pocket implant. Actually, the measured V_{TH} values increase from $0.21V$ for $L_g = 1.2\mu m$ to $0.27V$ for $L_g = 0.13\mu m$.

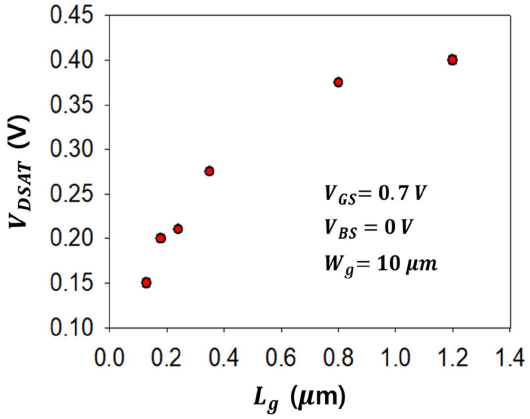

FIGURE 7. Extracted data of V_{DSAT} vs. L_g of BCT PD-SOI n-MOSFETs.

TABLE 1. Extracted terms in measured Y-intercept of (6).

L_g	Extracted $log(M_0)$	Extracted $-(S_I/m)(V_{DSAT}+E_g/q)$	Measured Y-intercept of $log(M-1)$
$0.13\mu m$	-4.660	-11.225	-15.886
$0.18\mu m$	-4.799	-11.713	-16.513
$0.24\mu m$	-5.143	-11.599	-16.742
$0.35\mu m$	-5.050	-12.162	-17.213
$0.8\mu m$	-4.952	-12.950	-17.903
$1.2\mu m$	-5.188	-12.828	-18.017

In addition, $log(M_0)$ can be obtained by subtracting the extracted value of $-(S_I/m)(V_{DSAT}+E_g/q)$ from the measured y-intercept of (6) in Fig. 6.

C. COMPARISON OF V_{DSAT} WITH M_0

Table 1 shows the influence of the extracted terms in (6) on the y-intercept of $log(M-1)$ in Fig. 6, which largely increases as L_g decreases. When V_{DSAT} decreases by $0.25V$ from $1.2\mu m$ to $0.13\mu m$ in Fig. 7, the value of $-(S_I/m)(V_{DSAT}+E_g/q)$ in (6) increases by 1.603, while $log(M_0)$ increases by only 0.528 in Table 1. In this scaling down of L_g, the influence of V_{DSAT} on the y-intercept increment of $log(M-1)$ in Fig. 6 is about 3 times greater than that of $log(M_0)$. This clearly proves that the increase of $M-1$ in the shorter channel in Fig. 6 is mainly caused by the decrease of V_{DSAT} in Fig. 7.

IV. ORIGIN OF L_G DEPENDENT V_{KINK}

Using (5) and (6) including the new parameters of V_{DSAT} and m, the V_{kink} relationship as a function of V_{Bi} and I_{DS} in (4) is modified by:

$$V_{kink} = \frac{m}{\eta}V_{Bi} + \frac{m}{S_I}\{log(I_{bo}) - log(I_{DS}) - log(M_0)\} + \frac{E_g}{q} + V_{DSAT} \quad (7)$$

Since V_{kink} is proportional to V_{DSAT} in (7), L_g dependence exhibiting a greater decrease at $L_g \le 0.35\mu m$ in Fig. 2 is similar to that of V_{DSAT} as shown in Fig. 7. In order to analyze the L_g dependence of V_{kink} using (7), it is important

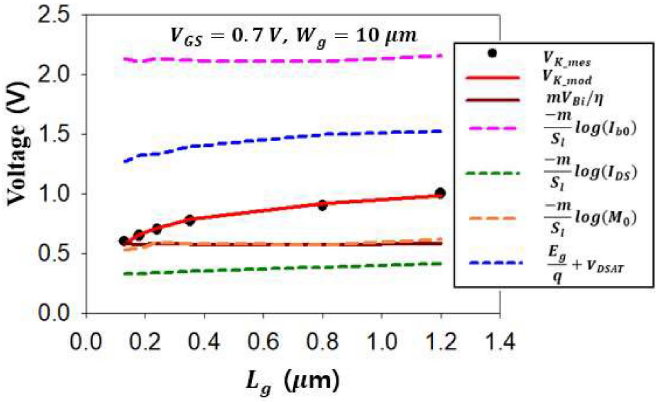

FIGURE 8. V_{K_mod} and V_{K_mes} vs. L_g graph plotted with the five terms that determine V_{kink} in (7). The I_{bo} term is multiplied by −1 to compare its magnitude with the others.

to know the exact V_{Bi} and the changes in each parameters at V_{kink} as L_g varies.

The parameters of I_{bo}, η, and m are determined by the y-intercepts and slopes of each straight lines extracted from Figs. 4 and 6. The I_{DS} data are also measured at V_{kink} for the BCT devices. The value of V_{Bi} at V_{kink} can be extracted by substituting these values and the measured V_{kink} at each L_g into (7). V_{kink} occurs at almost the same V_{Bi} in which V_{TH} begins to decrease regardless of L_g. All V_{Bi} values (average $V_{Bi\_avg} = 0.325V$) extracted for each L_g have a small deviation within 2.4%, which indirectly proves that the parameter values extracted from Figs. 4 and 6 are correct.

In Fig. 8, the modeled V_{kink} (V_{K_mod}) is calculated by substituting the values of I_{DS}, I_{bo}, η, m, M_0, and V_{DSAT} extracted at each L_g into (7) with V_{Bi_avg}, and is in good agreement with the measured V_{kink} in Fig. 3. In addition, in order to identify the main cause of L_g dependency of V_{kink}, the modeled individual terms of (7) are plotted to assess the influences of each components as L_g decreases in Fig. 8. This V_{kink} modeling approach leads to physical results with high accuracy, because most of the parameters in the V_{kink} equation of (7) are extracted through a direct linear fitting to measurement data from the BCT devices using theoretical equations of (1)–(6).

When L_g decreases from $0.35\mu m$ to $0.13\mu m$, the V_{kink} variation ΔV_{kink} owing to individual terms in (7) is the following: $\Delta V_{kink} = 0.008V$ due to the first term, $\Delta V_{kink} = -0.021V$ due to the second one, $\Delta V_{kink} = -0.018V$ due to the third one, $\Delta V_{kink} = -0.051V$ due to the fourth one, and $\Delta V_{kink} = -0.125V$ due to the reduction in V_{DSAT}.

Therefore, in this work, it is newly revealed that the decrease in V_{DSAT} resulting in about 60% out of total modeled ΔV_{kink} in $0.13\mu m \le L_g \le 0.35\mu m$ is the primary cause for a greater decrease in V_{kink} as L_g becomes shorter than $0.35\mu m$, and the increase of M_o is the next one. The third effect due to I_{DS} is relatively small because of the velocity saturation effect at shorter L_g.

V. CONCLUSION

To identify the cause of a greater decrease of V_{kink} in FB PD-SOI MOSFETs with shorter L_g than $0.35\mu m$, a V_{kink} equation as a function of V_{Bi} and I_{DS} obtained by combining the thermally-assisted M equation including V_{DSAT} and the body-source junction I-V equation is newly derived. Based on this equation, we confirmed that V_{kink} is affected by I_{DS}, I_{bo}, η, m, M_0, and V_{DSAT}, and these L_g dependent data are extracted by finding the slopes and y-intercepts of I_B vs. V_{BS} and $M - 1$ vs. V_{DS} in the BCT devices. By modeling V_{kink} using these data, it is newly discovered that the short-channel kink effect is mainly due to the reduction of V_{DSAT}.

REFERENCES

[1] K. Benaissa et al., "RF CMOS on high-resistivity substrates for system-on-chip applications," *IEEE Trans. Electron Devices*, vol. 50, no. 3, pp. 567–576, Mar. 2003, doi: 10.1109/TED.2003.810470.
[2] D. Leaderer and J.-P. Raskin, "New substrate passivation method dedicated to HR SOI wafer fabrication with increased substrate resistivity," *IEEE Electron Device Lett.*, vol. 26, no. 11, pp. 805–807, Nov. 2005, doi: 10.1109/LED.2005.857730.
[3] R. Stephan, M. Raab, H. Kuck, and H. Vogt, "Advanced SOI MOSFET for low voltage, low power and fast application," in *Proc. IEEE Int. SOI Conf.*, Oct. 1994, pp. 109–110, doi: 10.1109/SOI.1994.514270.
[4] S. S. Chen and J. B. Kuo, "An analytical CAD kink effect model of partially-depleted SOI NMOS devices operating in strong inversion," *Solid-State Electron.*, vol. 41, no. 3, pp. 447–458, Mar. 1997, doi: 10.1016/S0038-1101(96)00176-1.
[5] S. C. Lin and J. B. Kuo, "Temperature-dependent kink effect model for partially-depleted SOI NMOS devices," *IEEE Trans. Electron Devices*, vol. 46, no. 1, pp. 254–258, Jan. 1999, doi: 10.1109/16.737467.
[6] P. Su, S. K. H. Fung, H. Wan, A. Niknejad, M. Chan, and C. Hu, "An impact ionization model for SOI circuit simulation," in *Proc. IEEE Int. SOI Conf.*, Oct. 2002, pp. 201–202, doi: 10.1109/SOI.2002.1044475.
[7] K. K. Young and J. A. Burns, "Avalanche-induced drain-source breakdown in silicon-on-insulator n-MOSFETs," *IEEE Trans. Electron Devices*, vol. 35, no. 4, pp. 426–431, Apr. 1988, doi: 10.1109/16.2475.
[8] K. Lee and S. Lee, "Theory and analysis of kink effect in body contacted PD-SOI nMOSFETs," *J. Inst. Electron. Inf. Eng.*, vol. 56, no. 11, pp. 15–21. Nov. 2019, doi: 10.5573/ieie.2019.56.11.15.
[9] P. Su, K. I. Goto, T. Sugii, and C. Hu, "A thermal activation view of low voltage impact ionization in MOSFETs," *IEEE Electron Device Lett.*, vol. 23, no. 9, pp. 550–552, Sep. 2002, doi: 10.1109/LED.2002.802653.
[10] S. M. Sze, *Semiconductor Devices-Physics and Technology*, 2nd ed. Hoboken, NJ, USA: Wiley, 2002, pp. 109–114.
[11] N. Arora, *MOSFET Modeling for VLSI Simulation Theory and Practice*. Singapore: World Sci., 2007, pp. 475–477.
[12] N. D. Arora and M. S. Sharma, "MOSFET substrate current model for circuit simulation," *IEEE Trans. Electron Devices*, vol. 38, no. 6, pp. 1392–1398, Jun. 1991, doi: 10.1109/16.81631.
[13] B. Yu, C. H. J. Wann, E. D. Nowak, K. Noda, and C. Hu, "Short-channel effect improved by lateral channel-engineering in deep-submicronmeter MOSFET's," *IEEE Trans. Electron Devices*, vol. 44, no. 4, pp. 627–634, Apr. 1997, doi: 10.1109/16.563368.